THE ROLE OF BODY EXTENSION IN CEPHALOPOD LOCOMOTION

by JOHN A. CHAMBERLAIN, JR

ABSTRACT. The extension of the body outward from the aperture of the shell is a common behavioural trait of *Nautilus*, and presumably of most fossil ectocochliate cephalopods as well. In order to evaluate the possible contribution of body extension to ectocochliate locomotion, the hydrodynamic properties of body extension have been examined through tow-tank and flow-channel tests on shell models and body prostheses. Extension of the body reduces the drag generated by a swimming cephalopod. The extent of this reduction depends on how fully the body is extended, and on its posture relative to the flow. For most cephalopods this effect was probably small, but for some with compressed shells, and perhaps for *Nautilus*, an energy saving in the order of 25% may have been attainable. Extension of tentacles into the flow causes serious drag increases and can quickly overcome the beneficial effects of body extension. To minimize its drag, *Nautilus* retracts its tentacles when swimming fast, and in this aspect of its locomotory behaviour mirrors fish and squids, which do the same thing with their fins.

THE drag produced by a swimming animal depends not only on its general body shape, but also on details of its external anatomy. In the case of fossil cephalopods, a number of aspects of morphology besides basic shell geometry can be cited as possible contributors to drag production, and thus may be important in the locomotion of these animals. One of these factors is the extension of the body of the animal outward (backward actually) from the aperture. As it extends itself, an ammonoid or nautiloid can more readily interact with the flow and perhaps alter flow patterns around itself in a way that has some bearing on its progress through the water.

The significance of this kind of phenomenon has been of some interest to cephalopod palaeontologists in their attempt to understand the locomotory capacity and life styles of these animals. Schmidt (1930), who was the first student of cephalopods to develop quantitative data on shell flow properties, believed that body extension was undoubtedly an important hydraulic factor, and as a result was not confident that his drag measurements for empty shells were completely representative of the drag produced by the living animal. Geczy (1960) extended this notion by asserting that body extension was more important in drag production than many modifications of the shell. By drawing an analogy between the extended body of a cephalopod and the afterbodies of aircraft gun barrels, I have argued that body extension was probably not an important hydrodynamic factor for most shell forms (Chamberlain 1976). My main point was that in order to reduce drag significantly, afterbodies had to be about the same size as the barrel itself. I reasoned that the size of the extended body had to have been about the same as that of the shell and that the body should have extended forward into the umbilicus in order to produce a significant drag reduction in cephalopods. This clearly could not have occurred for most fossil cephalopods because evidence from buoyancy considerations, colour markings, pre-mortal epizoans, and general anatomy oppose this view.

While the gun-barrel analogy seems a cogent one, no hydrodynamic data exist that actually establish the hydraulic significance of body extension. The purpose of the present work is to fill this void. This paper reports results of experiments involving the use of plastic cephalopod shell models and wooden 'body' prostheses. These experiments are designed to develop data on flow patterns and drag coefficients of the shell and extended body. The work is directed toward resolving the question of the effectiveness of body extension in reducing the total drag acting on the animal, which I see as the crux of the debate on body extension. Other locomotory functions that may benefit from body extension, such as equilibrium and directional control, and such non-hydrodynamic functions as grasping, food capture, and visual enhancement, are not dealt with directly here.

[Palaeontology, Vol. 23, Part 2, 1980, pp. 445–461.]

METHODS

The approach employed here is based on the experimental procedures that I developed previously for studying the hydrodynamic properties of cephalopod shells (Chamberlain 1976). The procedure consists of two parts: (1) construction of shell models and body prostheses; and (2) testing the models in a tow tank and water channel.

I built two shell models using the template method of model construction described in Chamberlain (1969). One model has a compressed, moderately evolute form, while the other is depressed and involute (see text-fig. 1). Table 1 gives the dimensions of the two models and values for the descriptive parameters used to characterize the

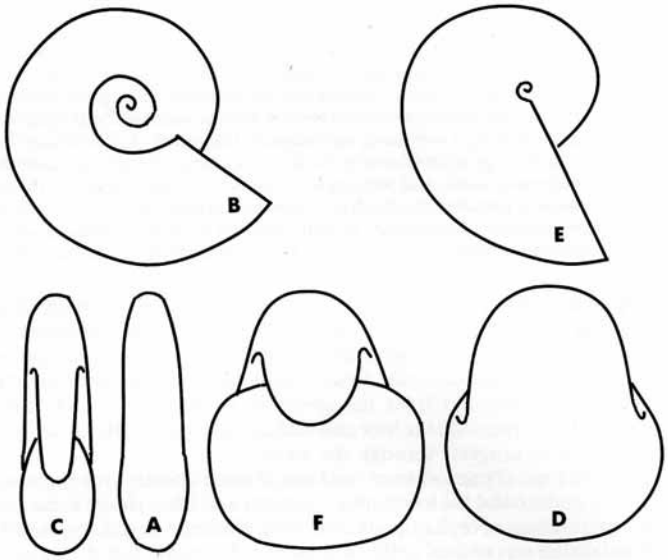

TEXT-FIG. 1. Plastic shell models used in this study. *A*, *B*, *C*: anterior, lateral, and posterior views of compressed model (model C). *D*, *E*, *F*: anterior, lateral, and posterior views of depressed model (model D). The terms anterior and posterior refer to orientation relative to the direction of motion of the swimming animal. No anatomical significance to these terms should be inferred.

TABLE 1. Geometrical parameters for shell models used in experiments. *W*, expansion rate; *D*, relative distance of whorls to the coiling axis; *S*, shape of whorl section; *F*, relative position of maximum whorl width. For algebraic definitions of geometrical parameters see Raup (1967) and Chamberlain (1976). Fineness ratio = maximum width of shell/shell diameter.

	General shape	Maximum diameter (cm)	Aperture width (cm)	Aperture height (cm)	Fineness ratio	Geometrical parameters			
						W	*D*	*S*	*F*
Model C	Compressed, moderately evolute	25·4	6·5	11·5	0·26	2·0	0·2	0·5	0·25
Model D	Depressed involute	12·7	10·5	8·5	0·83	3·5	0·07	1·25	0·4

geometry of coiled shells (see Raup 1967; Raup and Chamberlain 1967; Chamberlain 1976). The models were sanded and varnished to produce a smooth, mirror-like surface.

Extension of the body backward from the aperture was simulated by attaching realistically shaped body prostheses to the aperture of the shell models. Four such prostheses were fashioned from balsa-wood blocks for testing with the compressed model (model C), and one for testing with the depressed model (model D). Text-fig. 2 shows these prostheses. Except for the rear surface, which was left rough in three of the prostheses to simulate the irregularities made by the tips of the tentacles, each prosthesis was sanded and varnished to give it a smooth surface. In a general way, the shape of these prostheses is similar to the extended body of *Nautilus*, as shown in text-fig. 3. Each conforms to the whorl section of the shell model for which it is designed, and then tapers posteriorly. The prostheses differ from one another in size, degree of taper, and orientation relative to flow (see Table 2, text-fig. 2). However, the prostheses, being rigid, do not reproduce the elasticity of the skin in *Nautilus*, and thus would not be helpful in evaluating the possible damping effects of the skin on boundary-layer vorticity.

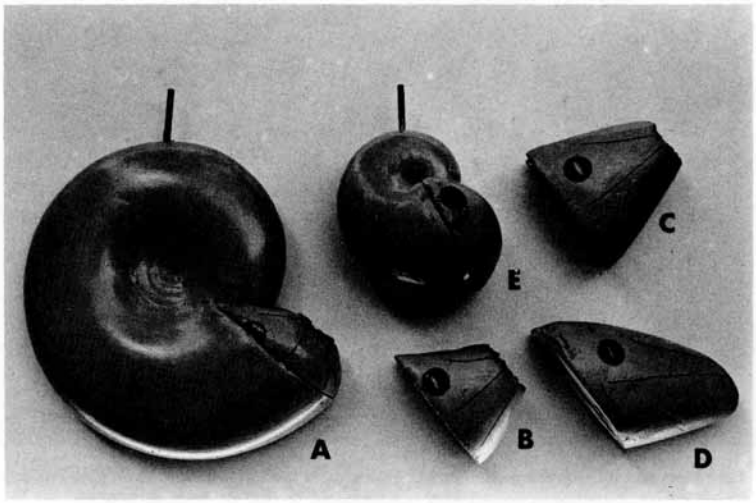

TEXT-FIG. 2. Body prostheses in lateral view. *A*: model C with small prosthesis (P1) attached to aperture. *B*: medium prosthesis (P2). *C*: large prosthesis (P3). *D*: streamlined prosthesis (P4). Prostheses 1–4 for use with model C. *E*: model D with prosthesis P5 attached to aperture.

TABLE 2. Dimensions of body prostheses. Prosthesis *P1–P4* for use with compressed model; prosthesis *P5* for use with depressed model. Length = length in cm along midline of prosthesis. Relative size = prosthesis length/maximum shell diameter. Taper = $\frac{1}{2}$ (width of aperture − width at rear of prosthesis)/length. Orientation relative to flow = angle in degrees between midline of prosthesis when attached to shell model and the direction of water flow around shell.

Body Prosthesis	length	Relative size	Taper	Orientation relative to flow
P1	4·5	0·18	0·28	45
P2	6·0	0·24	0·21	45
P3	9·0	0·35	0·17	45
P4	12·0	0·47	0·21	20
P5	3·0	0·24	1·08	30

TEXT-FIG. 3. Live specimen of *Nautilus pompilius* swimming in its tank at the New York City Aquarium. Degree of body extension shown here is equivalent to that of body prostheses.

Shell flow patterns were visualized by cementing dye crystals to the models and immersing them in a flow channel. Drag coefficients were determined from drag and velocity data obtained by testing the models in a tow tank (see Chamberlain 1976 for a more complete description of these procedures). The tests were performed with the flow channel and tow tank at Webb Institute of Naval Architecture, Glen Cove, N.Y.

The flow-channel and tow-tank tests were done using velocities likely to have been attained by fossil cephalopods. Analogy with *Nautilus* and other modern swimmers (Chamberlain and Westermann 1976) suggests the appropriate velocity range as 0–120 cm/sec, with most interest centring on the lower end of the range. The flow-channel tests were conducted at velocities of 30 cm/sec and 60 cm/sec; while the tow-tank tests covered a range of 35–110 cm/sec by making about twenty constant-velocity runs at small intervals within these extremes for each model configuration studied. Since the tow-tank carriage was designed for the high speeds of interest to naval architects and engineers, velocities lower than 35 cm/sec could not be attained with the apparatus used here.

To establish a basis for evaluating the hydrodynamic effects of body extension, the two shell models were first tested without body prostheses. Then prostheses were attached to the models and the tests repeated for each model-prosthesis configuration of interest. This procedure was followed in both tow-tank and water-channel experiments.

FLOW PATTERNS OF SHELL MODELS

The sketches in text-fig. 4, which are composites based on visual observation and photographs, show the flow field around each model. In each case the boundary layer remains attached to the surface of the model over the leading portion of the outer whorl, and then separates along the umbilical shoulder and the periphery of the aperture. Separation of the shell boundary layer at these locations induces a turbulent wake of considerable magnitude behind the shell. These results are consistent with my earlier determinations of cephalopod flow structure (Chamberlain 1976).

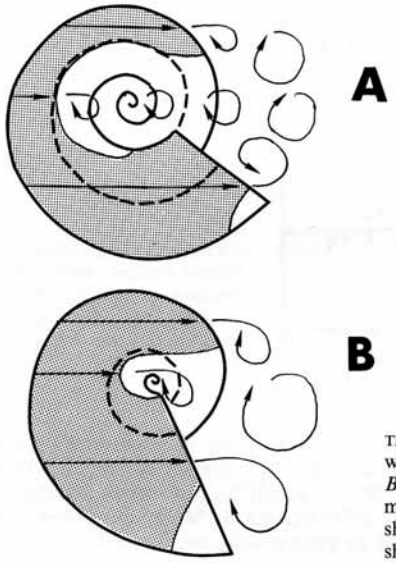

TEXT-FIG. 4. Flow fields of shell models without body prostheses. *A*: model C. *B*: model D. Area of boundary-layer attachment shown by stippling. Flow streamlines shown by solid lines. Umbilical shoulder shown by dashed line on outer whorl.

DRAG OF SHELL MODELS

Text-fig. 5 shows the results of the tow-tank tests plotted as drag coefficient (C_D) against velocity. Although drag coefficient is consistently lower for the compressed model, both models show the same kind of inverse relationship between drag coefficient and velocity. Two aspects of this relationship are worth noting: (1) drag coefficent diminishes rapidly as velocity increases at velocities below about 50 cm/sec; and (2) drag coefficient levels off and becomes nearly independent of velocity above about 50 cm/sec.

Drag-coefficient changes of the magnitude observed at low velocity in text-fig. 5 often occur when the position of boundary-layer separation shifts along the surface of an object. Fisher (1977), for example, observed this effect in the flow dynamics of the Pennsylvanian xiphosurian *Euproops danae*. In the present case, however, the reduction in drag coefficient occurs at Reynolds numbers ($Re \approx 2 \times 10^4$) for which this phenomenon would not normally be expected, and probably reflects nothing more substantial than the fact that the drag forces produced at these low velocities approximate the sensitivity of the dynemometer used to measure drag. The validity of these high drag coefficients at low velocity is thus suspect.

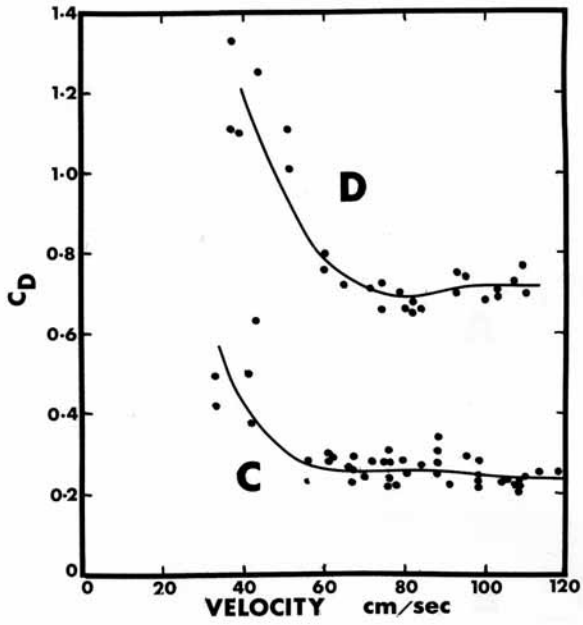

TEXT-FIG. 5. Drag coefficient (C_D) of shell models without body prostheses as a function of velocity. *C*, model C. *D*, model D. Each dot represents one constant-velocity tow-tank run. Curves fit by eye.

Above about 50 cm/sec, where drag forces are sufficiently large to be recorded accurately by the dynemometer, the drag coefficient—velocity curves in text-fig. 5 assume the flattened form typical of blunt, rounded bodies at Reynolds numbers of 10^4–10^5, and of the shell-drag coefficient curves that I obtained in previous experiments (Chamberlain 1976; text-fig. 6). Since model drag coefficients are virtually constant above 50 cm/sec, I calculated an average drag coefficient for each model. These average drag coefficients are given in Table 3. I would emphasize that, strictly speaking, the average values apply only to the velocity range of 50–110 cm/sec, although good hydrodynamic arguments exist for believing that the drag coefficient values given in Table 3 extend beyond these limits as well.

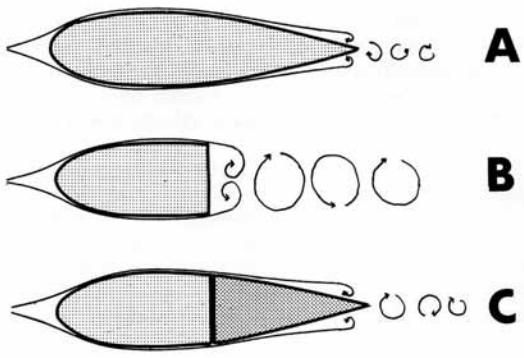

TEXT-FIG. 6. Flow fields around three bodies. *A*: fully developed fusiform body. Boundary layer remains attached to surface for considerable distance behind leading edge. Small wake. Low drag. *B*: underdeveloped body. Boundary layer is forced to separate prematurely at trailing edge. Wake large. High drag. *C*: underdeveloped body and afterbody. Boundary layer does not separate from trailing edge of leading body but remains attached over much of afterbody. Flow takes on characteristics of that for fully developed body.

TABLE 3. Average drag coefficients of smooth surfaced shell models. N, number of tow-tank runs; C_D, drag coefficient.

	Average		
	N	C_D	Std. Dev.
Model C	45	0·26	0·035
Model D	23	0·71	0·038

The probable swimming velocities of real animals the size of the models probably lie within the range to which the average drag coefficients most strictly apply (Chamberlain and Westermann 1976; text-fig. 7).

The marked difference in the drag coefficients of the two models noted in Table 3 is the result of difference in morphology, especially with respect to S (see Table 1). Because it is compressed (low S), model C has a smaller frontal area (projected area in direction of flow) relative to its size than does model D (compare text-fig. 1A and D). Thus, model C intercepts and redirects relatively less water than model D, and hence generates less drag. Model C also has a smaller aperture relative to its size than does model D—a feature which likewise derives from its compressed form (compare text-fig. 1C and F). Consequently, premature boundary-layer separation along the periphery of the aperture, and the drag elicited by this forced separation, is therefore less in model C. The hydrodynamic advantage gained by model D in having a small umbilicus is apparently overshadowed by the effects of these S-related aspects of shell geometry. This result is consistent with my previous findings concerning the relative contributions of W-, S-, and D-related drag components to total shell drag (Chamberlain 1976).

Table 4 compares models C and D with shell models of similar morphology tested previously. For model C and model 10, which differ mainly in the degree of shell compression (S), drag coefficient is seen to be much lower in the compressed specimen. The same relation is also seen in the data for the second group of specimens listed in Table 4, where the chief morphological variable is again shell compression. Drag-coefficient differences between specimens having the same compression (models 5 and 10) are due to differences in the degree of inflation (W). Model 5 has a somewhat higher drag

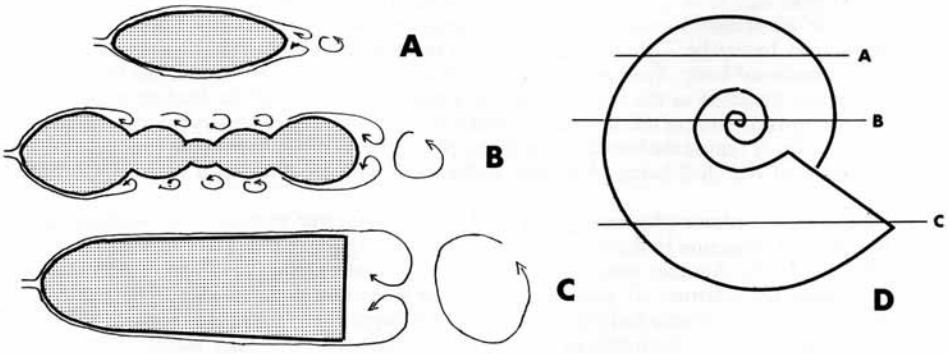

TEXT-FIG. 7. Flow over different parts of a cephalopod shell. *A*: flow across top of shell. *B*: flow in umbilicus. *C*: flow around bottom of shell and aperture. Flow is fully developed in *A*. Underdeveloped in *B* and *C*. *D*: lateral view of shell showing locations of cross-sections *A*–*C*. After text-fig. 5 of Chamberlain (1976).

TABLE 4. Average drag coefficients of smooth-surfaced specimens. Data for model 5, model 10, and *Nautilus pompilius* from Chamberlain (1976).

	Average C_D	Shell geometry			
		W	*D*	*S*	*F*
Model 10	0·57	2·0	0·2	1·0	0·23
Model C	0·26	2·0	0·2	0·5	0·25
Model D	0·71	3·5	0·07	1·25	0·4
Model 5	0·63	3·5	0·1	1·0	0·29
Nautilus pompilius	0·48	3·25	0·05	0·7	0·57

coefficient than model 10 because, being slightly more inflated, it has a relatively large frontal area and aperture. These results support my earlier assertion (Chamberlain 1976) that the shell morphology exhibiting the lowest over-all drag is probably one characterized by the smallest possible compression, inflation, and umbilicus (low S, low W, low D).

EFFECT OF BODY EXTENSION

The gentle curvature found in elongate, fusiform (fully developed) bodies allows the boundary layer to flow across the surface of the body with a minimal rate of momentum loss. As a result, the boundary layer remains attached to the surface for a considerable distance behind the leading edge of the object, thus ensuring that when the boundary layer does separate, the ensuing turbulence and drag are also minimal (text-fig. 6A). In contrast, the abrupt change in curvature of an underdeveloped body (text-fig. 6B) forces the boundary layer to separate before it would otherwise do so. This premature separation creates much turbulence and hence produces high drag forces. This situation can be greatly ameliorated by appending a second object, or afterbody, to the rear of the underdeveloped body (text-fig. 6C). If the afterbody is properly designed, i.e. if it is large enough to fill the dead-water region behind the first object and if it continues the curvature with no sharp gaps, the flow will be largely restored to the low turbulence, low drag condition of the fully developed body (text-fig. 6C).

A cephalopod shell is morphologically more complex than the simple bodies illustrated in text-fig. 6, but it nevertheless consists of regions that can be considered as fully developed or underdeveloped. In text-fig. 7, for example, it is clear that the upper part of the shell (text-fig. 7A) acts like a fully developed body. The gentle curvature of this part of the shell encourages the boundary layer to remain attached to the shell surface for some distance behind the leading edge (venter). However, the inward curve of the umbilical shoulder (text-fig. 7B), and especially the truncation at the aperture (text-fig. 7C) cause the boundary layer to separate prematurely from the rest of the shell. As a result of most of the shell being effectively underdeveloped, the drag on a cephalopod shell is relatively high.

The underdevelopedness of a cephalopod shell can be minimized through such modifications of shell geometry as reduction in the size of the umbilicus and aperture relative to the size of the shell (Chamberlain 1976). Another means to the same end would obviously be to extend the body backward from the aperture. If done properly, body extension could eliminate boundary-layer separation along the peristome and reduce the size of the stagnant region behind the shell, in the same way as for the afterbody illustrated in text-fig. 6C. Behaviour of this kind might be particularly important in those species where the details of shell form are specified by adaptive requirements other than drag minimization—a condition that may indeed be the general one because relatively few species appear to have shells close to the ideal for drag minimization.

FLOW PATTERNS OF SHELL MODELS AND BODY PROSTHESES

Text-fig. 8 shows the flow field set up by the shell models with attached body prosthesis. Comparison of text-fig. 8 with text-figs. 4 and 7 (see also text-fig. 4, and pl. 84 of Chamberlain 1976) demonstrates that the structure of the flow is essentially the same for both the shell alone and the shell with body. In both cases the flow separates along the umbilical shoulder of the models (shown in text-fig. 8 by distortion of dye streams on the flank of the outer whorl), and both elicit a wake of considerable magnitude (shown in text-fig. 8 by swirls of dye behind shell and in umbilicus). However, it is also clear from text-fig. 8 that the body prostheses do in fact act like the afterbody illustrated in text-fig. 6C. This is most readily apparent in text-fig. 8A where the dye streams emanating from the clusters of dye crystals on the body prosthesis are seen to streak out backward along the surface of the prosthesis. Premature boundary-layer separation at the aperture does not occur. Instead the boundary layer remains attached over most of the prosthesis. Note, however, that in contrast to the narrow, laminar streamlines at the leading edge of the shell, the dye streams on the prosthesis are wide, and evidently turbulent. Apparently by the time the boundary has reached the flank and rear of the prosthesis it has become turbulent and is ready to separate.

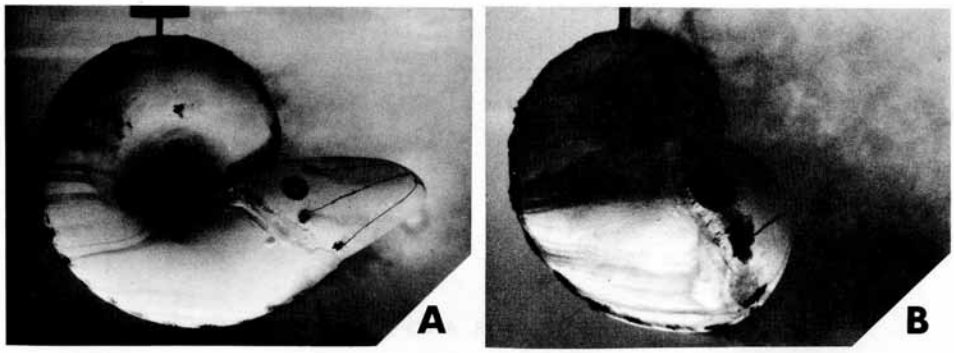

TEXT-FIG. 8. Flow fields of models with body prostheses attached to aperture. Flow velocity = 30 cm/sec. *A*: model C + prosthesis P4. *B*: model D + prosthesis P5. Dark objects along the venter, flank of the outer whorl, and on the side of the body prostheses are clusters of dye crystals.

In text-fig. 8B the afterbody effect is less obvious, although prosthesis P5 does fill a large volume behind model D. The dye released by the crystal clusters on prosthesis P5 appear to spread parallel to the peristome rather than backward as would be expected if flow were attached. Thus, it would appear that the boundary layer has already separated from the surface of the model despite the presence of the prosthesis. Evidently the major effect of the prosthesis in this case is to limit the scale of wake turbulence rather than to seriously modify boundary-layer behaviour. The difference between the two models in this respect undoubtedly derives from the differences between them in surface curvature. As suggested in text-fig. 9, attachment of the boundary layer in the case of model C is promoted by addition of the prosthesis because it continues the curvature of the model (text-fig. 9A). In contrast, prosthesis P5 (text-fig. 9B) does not continue the curvature of model D, but greatly magnifies it. As for the umbilical shoulder, momentum loss resulting from this rapid change in curvature is apparently severe enough to cause the boundary layer to stall and then separate at this location.

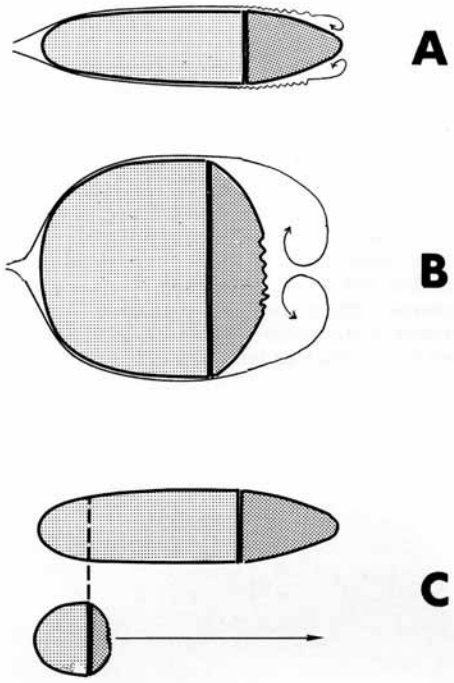

TEXT-FIG. 9. Flow patterns in region of aperture for shell models with prostheses. *A*: model C+prosthesis P4. Boundary layer is laminar at first and then develops vortices over the prosthesis. *B*: model D+prosthesis P5. Boundary layer separates due to curvature change at model-prosthesis juncture. Orientation of these cross-sections is the same as in text-fig. 7C. *C*: cross-sections drawn to same scale to emphasize that in terms of its flow properties, a depressed shell is equivalent to the anterior portion of a compressed shell, and that to produce a fully developed form, an animal with a depressed shell must extend its body much more than one with a compressed shell.

DRAG OF SHELL MODELS AND BODY PROSTHESES

Plots of drag coefficient against velocity for all model-prosthesis configuration tests give the same results as described above for the models alone, namely, drag coefficient is nearly independent at all but the lowest velocities attained with the test apparatus. Hence, I calculated drag coefficients for each model-prosthesis combination (Table 5). As in the case of the shell models alone, these drag coefficients should be considered as applying to the velocity range of about 50–110 cm/sec, but probably are valid for some distance beyond these limits also.

It seems clear from Table 5 that the addition of the prostheses to the shell models reduces drag coefficient. In view of the relatively minor differences between some test configurations, however, I performed *t*-tests on the data to determine if the observed differences are statistically meaningful. The results of these calculations are given in Table 6. It will be noted that some of the drag-coefficient differences are not statistically significant.

The data given in Tables 5 and 6 suggest some general rules about the functioning of body extension in ectocochliate locomotive hydrodynamics. The most obvious effect is to reduce the drag coefficient of the animal, and thus to enhance its hydrodynamic efficiency. In practical terms, this enhancement can be in the form of increasing velocity by the same relative amount that the drag coefficient is reduced, assuming that the energy saved is put back into the propulsive system. Alternatively, it can take the form of reducing propulsive output required to attain a given velocity with the concomitant saving of energy going to increase the animal's locomotory stamina, or into its general energy reserve.

TABLE 5. Average drag coefficients of shell models and body prostheses. N, number of tow-tank runs; C_D, drag coefficient. $\%C_D$ decrease $= 100 \times [(C_D \text{ of shell model}) - (C_D \text{ of shell model + prosthesis})]/(C_D \text{ of shell model})$. Fineness ratio at aperture = fineness ratio of apertural region of shell = maximum shell width/[(projected distance from venter to aperture in direction of flow) + length of body prosthesis, if present)]. A fully developed body has a fineness ratio = 0·20–0·24; underdeveloped body (too short) > 0·30. Overdeveloped body (too long) < 0·20.

Test configuration	N	Average C_D	Std. Dev.	$\%C_D$ Decrease	Fineness ratio at aperture
Model C	45	0·26	0·035	—	0·30
Model C+P1	20	0·22	0·018	15	0·28
Model C+P2	18	0·23	0·041	12	0·27
Model C+P3	17	0·24	0·025	8	0·24
Model C+P4	21	0·20	0·077	23	0·22
Model D	23	0·71	0·038	—	1·40
Model D+P5	18	0·64	0·083	10	1·00

The extent to which drag coefficient is reduced appears to be relatively small (about 10%) in most of the examples studied. Thus, the beneficial contribution of body extension to over-all locomotive capacity is likewise probably of minor consequence to the animal. This is to be expected in view of the fact that body extension in ectocochliates does not achieve a fully developed state for the shell-animal combination. The extended body does not completely fill the stagnant region behind the shell (text-fig. 8); it does not project into the umbilicus to prevent separation along the umbilical shoulder; nor does it necessarily inhibit separation at the peristome (text-fig. 8B). Despite these shortcomings of ectocochliate adaptive design, the data for model C+P4, where drag coefficient is reduced by 23% from the shell model alone, suggest that some ectocochliates may have been able to generate useful reductions in drag. As in the case of model C, those animals most likely to have done so, would have compressed shells because compressed shells have lower fineness ratios (see Table 1) and thus are more fully developed without body extension, and more likely to be fully developed when the body is extended (see text-fig. 9C; Table 5, column 6). As I have suggested previously (Chamberlain 1976), this would be especially true in high-shouldered oxycones because in such shells umbilical drag is small; the drag produced at the aperture is the major component of total shell drag. Reducing aperture drag by extending the body in these shells will therefore produce a much larger reduction in total drag than in the case of model C where, judging from its flow structure (text-fig. 8A), the umbilicus is a major drag contributor.

TABLE 6. Results of t-tests for determining significance of average C_D for the various test configurations studied. *, average C_D different at 95% confidence level; 0, average C_D not different at 95% confidence level.

	Model C + P1	Model C + P2	Model C + P3	Model C + P4	Model D + P5
Model C	*	*	0	*	
Model C+P1		0	*	0	
Model C+P2			0	*	
Model C+P3				*	
Model D					*

In principle, one would expect the magnitude of drag reduction to reflect the degree to which the body is extended. A protrusive body should produce a more fully developed form in the apertural region of a shell than a retracted body exposing only the tips of the tentacles. Yet, the data do not appear at first glance to support this expectation. Prostheses P1 through P4, while increasing uniformly in size relative to the shell (Table 2, column 2) and thus producing a progressively more fully developed form (Table 5, column 6), do not produce a correspondingly progressive reduction in drag coefficient (Table 5, column 5). P3, for example, elicits only an 8% drag-coefficient decrease (which is not statistically significant), whereas P1, which is much smaller than P3, gives a reduction nearly twice as large.

This apparent paradox can be understood in terms of the orientation of these prostheses relative to the flow. All are inclined to the flow: P1–P3 by 45°, and P4 by 20° (Table 2). This means that an increasingly large space develops between the trailing edge of the shell and prostheses as the size of the latter increases (text-fig. 10). As noted in text-fig. 10D, the effect of this gap on flow structure is to increase the turbulence around the rear of the prosthesis, rather like the tandem cylinder effect that I have described for gyrocones (Chamberlain 1976). The drag elicited will obviously depend on the degree of extension. When extension is pronounced, the space will be large and drag high, whereas the converse will hold when little extension occurs. This is precisely what we observe in the drag data for the sequence P1–P3. The beneficial effect of the large prosthesis (P3) is partially negated by the drag produced at the rear of the prosthesis so that the total drag loss is less. For P4 the orientation is only 20°—an inclination too small to produce this effect (note in text-fig. 8A that there is no noticeable diversion of the flow at the rear of the prosthesis). Thus, the full benefit of its large size can be realized, and it is observed to generate the greatest drag loss of all the examples studied.

We can now return to the original question of whether greater extension produces greater drag loss. P1 and P4 should be taken as the appropriate samples on which to base our arguments on this point because only in these two prostheses is the problem described above an insignificant one. P1 is too small to create a large gap, and P4 is too near parallelism with the flow to create a large gap. The drag

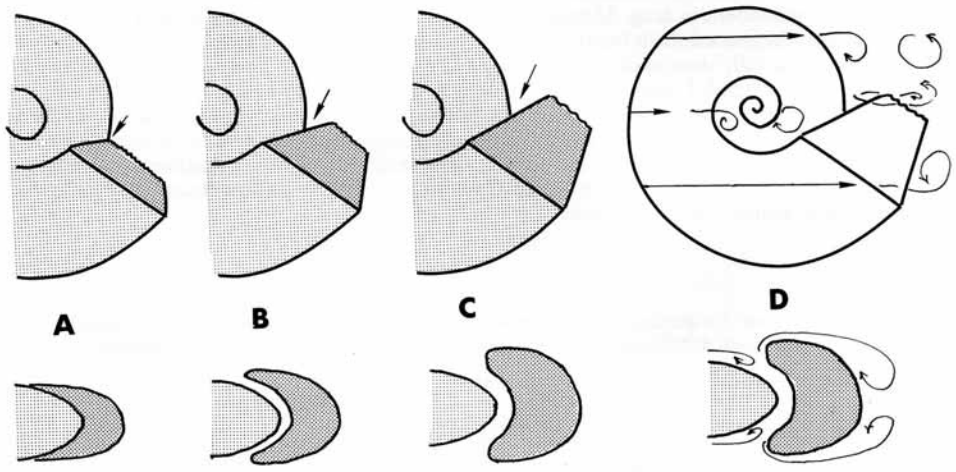

TEXT-FIG. 10. Effect of prosthesis orientation on flow structure for model C. Upper row shows profile at trailing edge of shell model. Lower row shows cross-section through shell model and prosthesis. Arrows point to space between trailing edge and prosthesis discussed in text. *A*: Pl. *B*: P2. *C*: P3. *D*: flow structure for model C+P3. Turbulence is enhanced by space between trailing edge of shell and prosthesis.

data for these two prostheses in Table 5 give results that seem consistent with our expectations; the larger prosthesis does indeed appear to produce a larger drag reduction. Table 6, however, shows that these results are not statistically significant. This can be taken in two ways: (1) the degree of extension has no measurable effect on drag loss; or (2) there is a relationship, but data in Tables 5 and 6 do not establish it firmly. I prefer the second alternative. I believe that the key here is the unusually high standard deviation for the average drag coefficient of P4 (see Table 5). The reason for this anomalously high standard deviation is shown in text-fig. 11. P4 is the only prosthesis in which drag coefficient can be identified as varying appreciably with velocity. By assuming that drag coefficient is independent of velocity, which is implicit in computing an average drag coefficient, this velocity-related variation is expressed as dispersion around the mean drag coefficient, resulting in a high standard deviation.

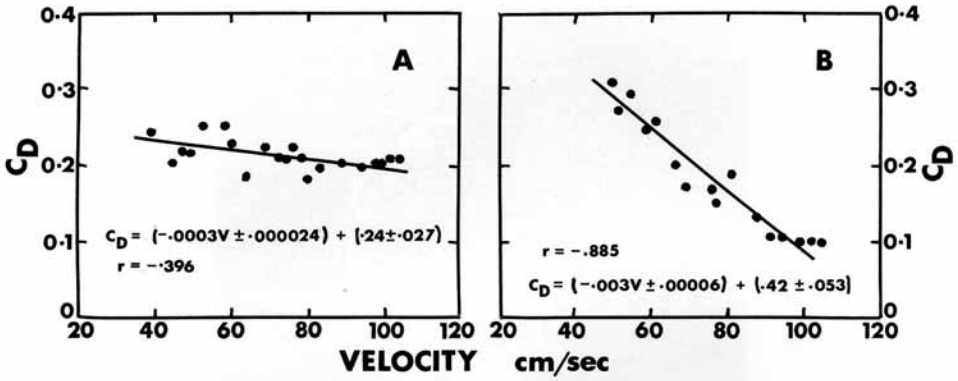

TEXT-FIG. 11. Drag coefficient as a function of velocity for two body prosthesis configurations. *A*: model C + Pl. *B*: model C + P4. Each dot represents one constant-velocity tow-tank run. Linear regression lines fitted to data. Regression equations shown on plots. C_D, drag coefficient; V, velocity in cm/sec; r, correlation coefficient.

A better way to treat the data in this case is to analyse the relationship between drag coefficient and velocity. I fitted linear regression lines to the data for both prostheses. The equations for these lines and their correlation coefficients (which are significant at the 95% level according to the procedure given by Till 1974, pp. 86, 87), are shown in text-fig. 11. The slopes and intercepts of the two lines are clearly different, which implies that the hydrodynamic effect of the two prostheses is probably also different, even though the means of the two data sets cannot be statistically distinguished. Thus, from text-fig. 11 it seems that for compressed ectocochliates (and perhaps for others as well) increased body extension may enhance drag reduction, at least at high velocities.

One implication of these considerations is that an ectocochliate may elevate its performance by extending its body as far as possible, especially at high velocity. But in doing so, it must take care to align itself parallel to the flow so that it avoids forming gaps behind the trailing edge of the shell. Proper posture is critical. The specimen shown in text-fig. 3 seems to have achieved this condition, but it would be unwarranted to assume that the data given in text-fig. 11 accurately reflect the benefit this *Nautilus* acquires by this behaviour. The animal's velocity was not measured and this may be of some significance as text-fig. 11 implies, but more importantly, neither shell model nor any of the prostheses incorporate the anatomical details seen in *Nautilus*. How much *Nautilus* profits energetically from such behaviour must remain uncertain until more sophisticated analysis is accomplished.

THE EFFECT OF TENTACLE EXTENSION

Most aquatic animals exhibit several different swimming styles, each of which is used for a specific purpose. Many squids and teleost fish, for example, rely on fin propulsion at slow speeds, but fold their fins against their bodies to reduce drag and conserve energy at high speed (Zuev 1966; Trueman and Packard 1968; Hertel 1966). Ectocochliates may also show a multiplicity of swimming styles. *Nautilus* certainly does. During its peak locomotory periods, the body is extended and the tentacles held in the tapering mass shown in text-fig. 3. When swimming at moderate speeds near the bottom, two tentacles are often extended downward to retain tactile contact with the substrate. At slow speeds, especially when attempting to locate food or to grasp some object, a number of tentacles are extended outward in a search web (see text-fig. 12).

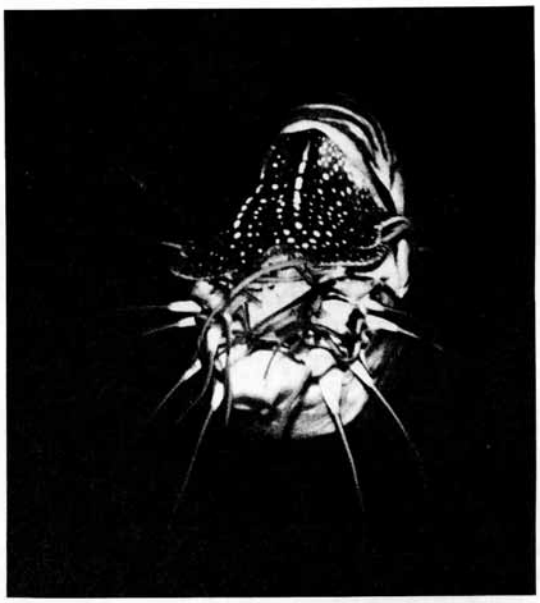

TEXT-FIG. 12. *Nautilus* taking shrimp. Slow movement, tentacles deployed in search web. Wire holding shrimp is seen descending from upper left corner.

It is interesting to reflect on the role of tentacle extension in locomotion and expecially on the additional drag that extended tentacles create. To do this, recourse to experiments like the present ones is fortunately not necessary because an adequate theory exists for the prediction of tentacle drag.

The drag on a single fully extended tentacle can be estimated if we assume that the tentacle is a straight, circular cylinder inclined at some angle of attack (θ) to the flow. Text-fig. 12 suggests that this assumption is not unrealistic. Furthermore, we will say that the tentacle sheath is operating in the separated flow near the shell and hence can be neglected as far as its drag is concerned. Judging from the positions of the sheaths in text-fig. 12, this too is a reasonable assertion. This assumption also has

the advantage that we need not concern ourselves with interference drag at the tentacle-body contact. The normal force (F_N) acting on such a tentacle will be given by:

$$F_N = \tfrac{1}{2}\rho V^2 A C_{D_c} \sin^2 \theta \qquad \text{Eq. 1}$$

where ρ is water density; V is swimming velocity; A is frontal area; and C_{D_c} is the drag coefficient of a circular cylinder held perpendicular to the flow (see Taylor 1952; Hoerner 1965). Substituting $A = dh$ (diameter·height) and drag force (D_F) $= F_N \sin \theta$, we can write:

$$D_F = \tfrac{1}{2}\rho V^2 dh C_{D_c} \sin \theta \qquad \text{Eq. 2}$$

Since C_{D_c} for a perpendicular cylinder $\approx 1{\cdot}0$ in the present Reynolds number range; $\rho = 1{\cdot}027$ gm/cm^3; and since tentacle length ≈ 9 cm, tentacle diameter $\approx 0{\cdot}3$ cm, and $\theta \approx 135°$, in the adult animals observed at the New York Aquarium, equation 2 becomes:

$$D_F = 0{\cdot}98 \text{ gm/cm } V^2. \qquad \text{Eq. 3}$$

We can now calculate the drag force produced by this tentacle (or any number of similar tentacles by simply multiplying the right side of equation 3 by this number), and compare the result with the drag generated by the shell and extended body. Text-fig. 13 shows the outcome of these computations expressed in terms of drag coefficients. The parameter plotted on the ordinate ($\%\Delta C_D$) should be understood as the change in drag coefficient produced by a fully extended body with a specific number of extended tentacles (read on the abscissa) relative to the drag coefficient of the empty shell, i.e.

$$\%\,\Delta C_D = 100 \cdot [(C_{D_{s+b+t}}/C_{D_s}) - 1]$$

where C_{D_s} is shell drag coefficient; and $C_{D_{s+b+t}}$ is the drag coefficient of the shell + body + tentacle combination. A negative value for this parameter means that $C_{D_{s+b+t}}$ is less than C_{D_s}, while a positive value means that it is greater than C_{D_s} (remember that hydrodynamic efficiency increases as $\%\,\Delta C_D$ takes on increasingly negative values). The calculation of per cent drag coefficient change is based on a C_{D_s} for *Nautilus* of 0·5 (Chamberlain 1976), and incorporates the assumption that correct body extension (without protrusive tentacles as in text-fig. 3) provides a reduction of about 25% in total drag ($-0{\cdot}25$ on ordinate in text-fig. 13). While the present tow-tank data cannot be used to pin-point the effect of body extension for *Nautilus*, as noted above, it seems unlikely in view of the similarity in the degree of body extension between model $C+P4$ and the *Nautilus* in text-fig. 3, that *Nautilus* can achieve a drag reduction in excess of 25%. It may well be less, but I think that 25% represents a reasonable upper limit, and so I have chosen this value as a basis for constructing the plot in text-fig. 13. If the true reduction is less than 25%, the *Nautilus* curve will simply be shifted downward by the difference between the actual value and my 25% estimate.

The main point made in text-fig. 13 is that tentacle drag is an important component of total drag. Extending only two tentacles while swimming, as *Nautilus* often does, results in a drag increase of

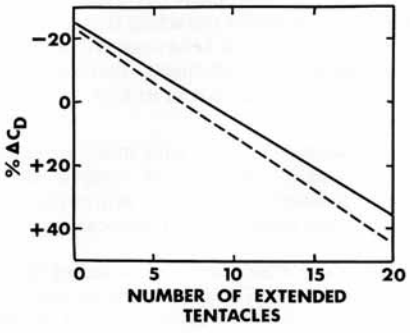

TEXT-FIG. 13. Per centage change in drag coefficient ($\%\,\Delta C_D$) caused by extension of tentacles outward from body relative to drag coefficient of empty shell. When number of extended tentacles = 0, $\%\,\Delta\, C_D$ = change in C_D of shell alone due only to body extension. See text for further discussion. Solid line—adult *Nautilus* as described in text. Dashed line—model C+P4 with degree of tentacle extension as for *Nautilus*.

about 7%, while extending ten tentacles as in text-fig. 12 results in about 5% more drag than if body and tentacles were completely retracted into the shell. When twenty tentacles are extended drag is about 37% greater than if the animal were completely retracted, and 62% greater than if its body were properly extended. Surely, it cannot be a surprise that as a *Nautilus* increases its speed it retracts its tentacles. This aspect of *Nautilus* behaviour thus seems to derive from the same respect for conservation of propulsive energy that impels fish and squids to fold their fins at high speed. There is, however, one important difference between *Nautilus*, fish, and squids in this regard. Because of its relatively poor eyesight (see Packard 1972), *Nautilus* apparently relies in many situations on the sensitivity of its tentacles to provide information about its surroundings. When the tentacles must be retracted to maximize speed, *Nautilus* would seem to lose a significant portion of the sensory input needed to judge position, direction, and speed, perhaps to the point where an animal is effectively swimming blindly at peak speeds. Qualitative observations made on five specimens at the New York City Aquarium suggest that at its highest speeds, *Nautilus* 'crashes' more frequently into obstacles than when swimming slowly. With their anterior, camera-type eyes, fish do not have this problem (although in a few species, like angelfish, some fins may have a tactile function). Squids seem to be intermediate. Like fish they have camera eyes, but like *Nautilus* the eyes are far back on the body. Undoubtedly, the same considerations apply to fossil ectocochliates. They too may have had difficulty in control at high speed.

The dashed line in text-fig. 13 is for model $C+P4$ with hypothetical extended, cylindrical tentacles, for which the tentacles bear the same relative size (with respect to shell) as for *Nautilus*. It shows that in animals with compressed shells, the effect of tentacle extension is even more severe than for *Nautilus*. This is because the drag coefficients of these shells are small so that tentacle drag makes up a larger fraction of total drag.

SUMMARY

Studies of the hydrodynamic properties of body extension in ectocochliates by tow-tank and flow-visualization experiments on scale models of shells and cephalopod bodies allow a number of conclusions to be drawn:

1. Extension of the body from the aperture produces a small ($\sim 10\%$), but measurable decrease in drag. In compressed shells, and perhaps in a few others, e.g. *Nautilus*, the change may have been as high as $\sim 25\%$. Thus, body extension may have had an important beneficial effect in the locomotion of some ectocochliates, but for most was probably of relatively minor significance.
2. The extent of drag reduction produced by body extension depends on posture. To be most effective, the body must be extended parallel to the flow direction (direction in which animal swims), extended as fully as possible, and extended so that no gaps are allowed to form between the body and trailing edge of the shell. *Nautilus* (see text-fig. 3) is capable of this kind of extension.
3. Extending tentacles outward into the flow as *Nautilus* often does (see text-fig. 12) can greatly increase drag, and completely overcome the beneficial effect of the extended body. In *Nautilus* this problem is minimized by retracting the tentacles into their protective sheaths during periods of peak locomotory activity. This behaviour is analogous to fin folding seen in many fish and squids at high speed. But unlike fish and squids, *Nautilus* evidently loses a significant portion of its spatial sensory input in this process, so that at its high speed, *Nautilus* is much less adept than fish or squids are at theirs.

It would appear that, as with many scientific controversies, the hydrodynamic effect of body extension actually represents a compromise between opposing views; in this case, of such researchers as Schmidt and Geczy who envisioned body extension to be of major importance in drag production, and myself when I advocated the antithesis in my 1976 paper.

Acknowledgements. I am grateful to the staff of Webb Institute of Naval Architecture, and especially to Rear Admiral C. N. Payne U.S.N. (Ret.), president, and Professor E. V. Lewis, director of research, for allowing me to use their facilities. I am also greatly indebted to Professors N. A. Hamlin and L. W. Ward (both of Webb

Institute) for their guidance and friendly co-operation during the course of the experiments. I thank Dr. G. D. Ruggieri, S.J., director of the New York City Aquarium, for permitting me to study the *Nautilus* specimens in his care. The assistance of A. A. S. Chamberlain, R. B. Chamberlain, and A. Shapiro (Brooklyn College) was instrumental in completing the experimental portion of the work. This research was supported by a grant from the Research Foundation of the City University of New York.

REFERENCES

CHAMBERLAIN, J. A., JUN. 1969. Technique for scale modelling of cephalopod shells. *Palaeontology*, **12,** 48–55, pl. 7.

—— 1976. Flow patterns and drag coefficients of cephalopod shells. Ibid. **19,** 539–563, pl. 84.

—— and WESTERMANN, G. E. G. 1976. Hydrodynamic properties of cephalopod shell ornament. *Paleobiology*, **2,** 316–331.

FISHER, D. C. 1977. Functional significance of spines in the Pennsylvanian horseshoe crab *Euproops danae*. Ibid. **3,** 175–195.

GECZY, B. 1960. On the way of life of the Neoammonoids. *Földt. Közl.* **90,** 200–203.

HERTEL, H. 1966. *Structure, form, and movement*. Reinhold, New York. 251 pp.

HOERNER, S. F. 1965. *Fluid dynamic drag*. The author, Midland Park, New Jersey. 432 pp.

PACKARD, A. 1972. Cephalopods and fish: the limits of convergence. *Biol. Rev.* **47,** 241–307.

RAUP, D. M. 1967. Geometric analysis of shell coiling: coiling in ammonoids. *J. Paleont.* **41,** 43–65.

—— and CHAMBERLAIN, J. A., JUN. 1967. Equations for volume and center of gravity in ammonoid shells. Ibid. 566–574.

SCHMIDT, H. 1930. Über die Bewegungsweise der Schalencephalopoden. *Z. Paläont.* **10,** 136–143.

TAYLOR, G. 1952. Analysis of swimming of long and narrow animals. *Proc. R. Soc.* **217A,** 158–183.

TILL, R. 1974. *Statistical methods for the earth scientist*. Halsted Press, New York. 154 pp.

TRUEMAN, E. R. and PACKARD, A. 1968. Motor performances of some cephalopods. *J. exp. Biol.* **49,** 495–508.

ZUEV, G. V. 1966. Characteristic features of the structure of cephalopod molluscs associated with controlled movements. *Ekologo-morfolo-quicheskie issledovanniya nektonnykh zhivotnyk, Kiev*. Spec. Publ. **14.** Fish Res. Bd. Canada, Transl. Ser. No. 1011.

JOHN A. CHAMBERLAIN, JR.

Dept. of Geology
Brooklyn College of the City University of New York
Brooklyn
N.Y. 11210, U.S.A.

Manuscript received 15 May 1979